(Received 13 September 2024, Accepted 16 October 2024, Scheduled 6 November 2024)

A 2-Port High Isolation Millimeter Wave Dual-Band Antenna Based on SIW Back-Cavity Slot

Mingming Gao[1,2], Chang Ge[1,2,*], Jingchang Nan[1,2], Chunli Liu[1,2], Hongliang Niu[1,2], and Hang Yuan[1,2]

[1]*Liaoning Technical University, China*
[2]*Liaoning Key Laboratory of Radio Frequency and Big Data for Intelligent Applications, China*

ABSTRACT: To enhance the transmission rate and bandwidth utilization of Multiple-Input Multiple-Output (MIMO) communication systems, a dual-band MIMO antenna for millimeter waves is proposed, which is based on a substrate-integrated waveguide (SIW) and fed by a 50 Ω microstrip line. To achieve the dual-band performance, it employs a modified dual P-shaped slot instead of the conventional single P-shaped slot. The modified slot antenna generates dual-frequency radiation by exciting the primary and mixed modes in the circular resonant cavity. To improve the channel capacity of the system, the antenna is formed into a 2-element antenna, and the isolation of the antenna is improved by pattern diversity and defected ground structure (DGS). The antenna's prototype is fabricated using a standard printed circuit board (PCB) process. The antenna's dimension is $20 \times 18.9 \times 0.508\,\text{mm}^3$. Measured results show that the impedance bandwidth of the antenna is about 26.7 GHz–27.9 GHz and 37.95 GHz–40.92 GHz with peak gain of 5.63 dBi and 6.35 dBi, respectively. In addition, the isolation degree is greater than 30 dB, the envelope correlation coefficient (ECC) less than 0.0002, and the diversity gain (DG) greater than 9.995. The antenna shows the advantages of low profile, dual-frequency radiation, and high isolation characteristics, which are well suited for millimeter-wave wireless communication systems.

1. INTRODUCTION

With the rapid advancement of communication technology and the extensive deployment of millimeter-wave frequency bands, an increasing number of frequency bands have captured the attention of researchers. In contrast to microwave bands, millimeter-wave bands offer richer spectral resources and larger bandwidth, crucial for satisfying the increasing demand for wireless communications [1, 2]. To meet the requirements of multi-band communication systems and enhance data throughput, dual-band Multiple-Input Multi-Output (MIMO) antennas have garnered significant attention from researchers. Millimeter-wave dual-frequency MIMO technology integrates the high-speed, low-latency characteristics of millimeter-wave communication with the advantages of large communication capacity and high frequency utilization in MIMO multi-antenna technology, making it a key technology for 5G communication [3].

In the realm of dual-band MIMO antennas, scholars have conducted extensive research on methods to enhance isolation. However, as the number of antennas in MIMO systems increases, ensuring effective isolation between them becomes more difficult. Furthermore, multi-band MIMO antennas exhibit more bands decoupling and more intricate coupling relationships than their single-band counterparts. Commonly employed techniques to enhance isolation include etched defected ground structures (DGSs), parasitic elements, electromagnetic band gap (EBG) structures, and neutralization line techniques [4–15]. An 8-element dual-band MIMO antenna operating in 3300–4200 MHz and 4800–5000 MHz is proposed in [6]. Mutual coupling is effectively reduced by a T-shaped decoupled stub structure. Ref. [7] realizes dual-band function by etching L-shaped slots on the radiating patch and uses a decoupling structure consisting of a cross-shaped metal strip to improve isolation. Ref. [8] proposes a novel dual-band 4-shaped printed MIMO antenna of two elements. The isolation between the two elements is more than 17 dB in the low band after DGS is used. A miniaturized 2×2 dual-band MIMO antenna operating in the frequency bands from 2.408 to 2.776 GHz and 4.96 to 5.64 GHz is proposed in [9]. The mutual coupling effect between the radiating units is minimized by partial step grounding (PSG) and by polarization diversity, and the measured isolation is greater than 21 dB. A dual-band 2×2 MIMO antenna based on a half-mode substrate-integrated waveguide (HMSIW) is proposed in [10]. A small neutralization line in the center of the antenna is used to improve the isolation of the antenna, and the minimum isolation of the two bands is greater than 35 dB. Cross-shaped strips above the substrate are symmetrically added among the MIMO elements to enhance the ports' isolation in [12]. The metasurface with negative permeability is designed and achieves significant mutual coupling reduction over the entire bandwidth in [13].

Almost all of the antennas in the above literatures operate in lower frequency bands. To address the need for high-speed data transmission and low-latency communication in current systems, [14] achieved resonance at 28 GHz and 38 GHz with a minimum port isolation of 28 dB by employing polarization diversity using an E-shaped patch featuring an H-shaped slot. Ref. [15] presents a 2-element millimeter band MIMO antenna

* Corresponding authors: Chang Ge (2054892220@qq.com).

operating at 27 GHz and 39 GHz with more than 25 dB isolation by using pattern diversity. However, the above literature uses microstrip lines to design the cells of the dual-band MIMO antenna, which has a high radiation loss compared to the SIW technique and is not an ideal choice in millimeter-wave RF devices [16, 17]. And the commonly used decoupling methods for millimeter wave multi-band or wide-band decoupling design will be more difficult, thus how to design a low-coupling, multi-band MIMO antenna is a challenge.

Therefore, this paper presents the design of a miniaturized, low-profile, millimeter-wave dual-band MIMO antenna with high isolation, employing a substrate integrated waveguide (SIW) back-cavity structure. An improved dual P-shaped slit is etched on the upper surface of the SIW circular back-cavity to overcome the limitation of single-band operation, enabling dual-band radiation and enhancing antenna efficiency. The method of DGS and pattern diversity is employed to arrange two antenna units in parallel, forming a high isolation dual-band MIMO antenna. Experimental results demonstrate that the antenna operates effectively at 26.7 GHz–27.9 GHz and 37.95 GHz–40.92 GHz, with relative bandwidths of 4.4% and 7.5%, respectively. The antenna achieves peak gains of 5.63 dBi and 6.35 dBi in the two bands and maintains an isolation degree exceeding 30 dB.

The paper is organized as follows. Section 2 discusses the structure of a dual-band MIMO antenna and analyzes the working principle of the antenna to achieve dual-band radiation and high isolation. Section 3 discusses the results of the study and compares them with the existing research results. Section 4 discusses the conclusions and future perspectives.

2. ANTENNA DESIGN AND ANALYSIS

2.1. Design of Dual-Band Antenna Units

The dual-band antenna unit is designed on a single-layer dielectric substrate (Rogers 5880) with specific material characteristics: a dielectric constant (ε_r) of 2.2, dielectric loss tangent (tanδ) of 0.0009, and thickness of 0.508 mm. Within the dielectric substrate, a SIW circular cavity is formed using metal vias in Fig. 1.

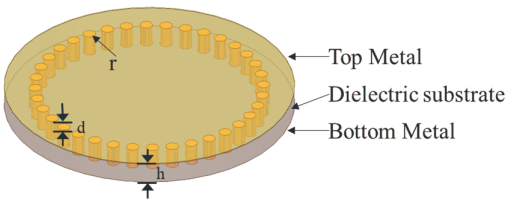

FIGURE 1. SIW circular resonant cavity.

For the low-profile SIW circular resonant cavity, the electric field strength can be approximated as uniformly distributed along the z-direction. Under this assumption, the resonant frequency of its characteristic mode can be obtained from Equation (1) [18].

$$f_0 = \frac{c_0}{2\pi\sqrt{\mu_r\varepsilon_r}} \cdot \frac{p_{nm}}{R'} \tag{1}$$

where f_0 is the resonant frequency; c_0 is the speed of light in vacuum; ε_r and μ_r are the relative permittivity and permeability of the substrate, respectively; P_{nm} stands for the m-square root of the first type of nth-order Bessel function; R' is the equivalent radius of the SIW circular resonant cavity, which can be approximated by the following Equation (2):

$$D_{eff} = 2 \times R_0 - \frac{d^2}{0.95p} \tag{2}$$

where R_0 is the radius of the SIW circular cavity, D_{eff} the equivalent diameter of the SIW circular cavity, d the diameter of the metal through-hole, and p the distance between the centers of two adjacent through-holes. P and d should satisfy the two conditions of $p < 2d$ and $d/\lambda_0 < 0.1$ (λ_0 is the resonance wavelength in the free space) in order to reduce the leakage of electromagnetic energy and to maintain the stability of the structure.

Inside the SIW circular resonant cavity, the gray shading surrounded by the black solid line represents a modified dual P-shaped slit radiating unit etched out by a PCB process on the upper surface of the SIW cavity, which consists of a longitudinal slit offset from the central axis and two portions of the toroidal slits that are cropped by this longitudinal slit in Fig. 2, wherein the inner and outer diameters of the portions of the cut large toroidal slits are r_2 and r_1, respectively, and the inner and outer diameters of the portions of the small toroidal slits are r_5 and r_4, respectively. The longitudinal slit extends out of the toroidal slit by a length of n_1, and the distance of the longitudinal slit away from the central axis of the SIW cavity is m_1. The radii of the toroidal slits follow the approximate formulas described in Equation (3) [19]:

$$f = \frac{1.4c}{2\pi r_e\sqrt{\varepsilon_e}} \tag{3}$$

where $r_e = (r_1 + r_2)/2$ is the equivalent radius of the circle, $\varepsilon_e = (\varepsilon_r + 1)/2$ the equivalent permittivity at the slit, and f the operating frequency of the antenna.

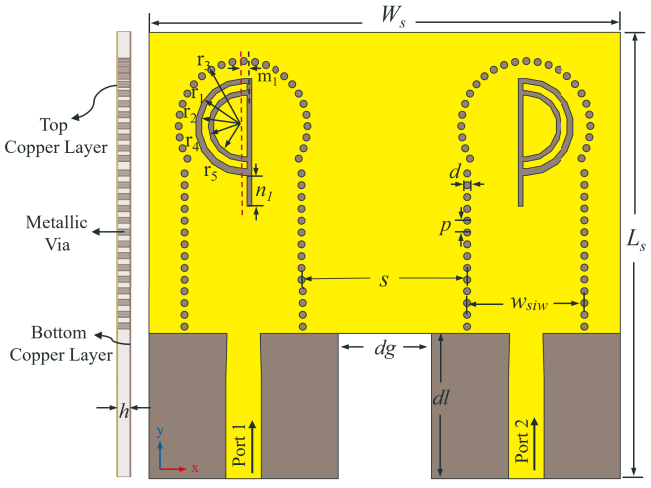

FIGURE 2. Configuration of the proposed antenna.

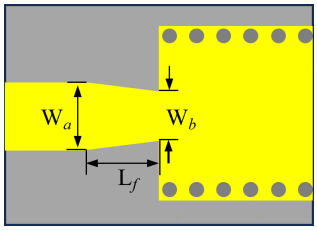

FIGURE 3. SIW to microstrip conversion structure.

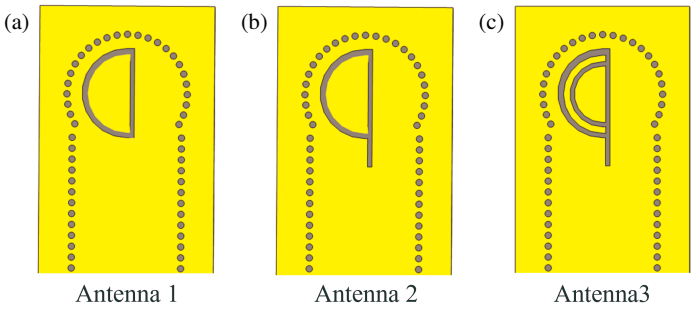

FIGURE 4. The evolution of the proposed antenna from Antenna 1 to Antenna 3.

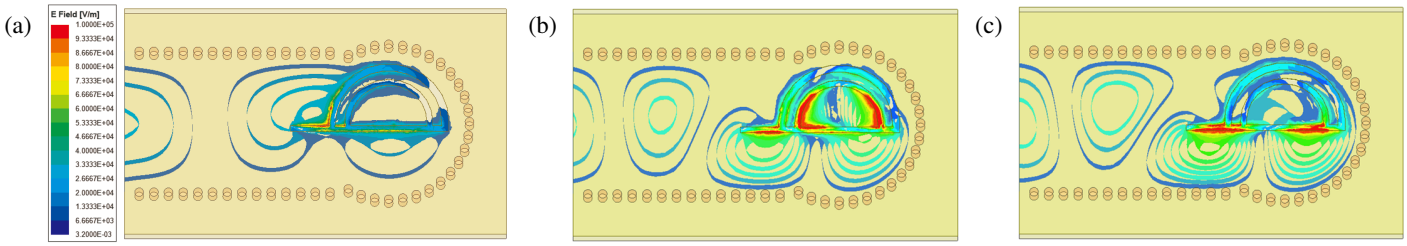

FIGURE 5. The energy distribution of the antenna electric field (a) 27.5 GHz; (b) 38.5 GHz; (c) 39.5 GHz.

Meanwhile, addressing the antenna connection testing issue necessitates designing a tapered transition structure to facilitate the conversion between SIW and 50 Ω microstrip in Fig. 3. This structure offers advantages such as simplicity, ease of implementation, low return loss, and broad bandwidth.

The equivalent impedance of the SIW_{TE10} mode can be obtained from Equation (4) [20].

$$Z_e = \frac{\pi h}{2W_{eff}} \frac{\eta_0}{\sqrt{\varepsilon_r \left[1 - \left(\frac{\lambda}{2W_{eff}}\right)^2\right]}} \tag{4}$$

where W_{eff} is the equivalent rectangular waveguide width. The equivalent impedance Z_e is substituted into the formula for solving the width of the microstrip line, and the width W_b of the microstrip line corresponding to Z_e can be solved to be 1.4 mm. The optimized 50 Ω microstrip line has a width W_a of 1.5 mm, and the length of L_f is 1.9 mm approximating 1/4 wavelength in vacuum at 39 GHz. Finally, it is optimized by HFSS simulation to make the best match between microstrip and SIW.

2.2. Operating Principle of Antennas

Fig. 4 illustrates the design concept of the antenna unit, demonstrating how the SIW circular resonant cavity evolves into a dual-band radiating antenna. Initially, a closed semicircular slit is etched inside the SIW resonant cavity, offset vertically from the central axis by a certain distance to modify the antenna's radiation characteristics. Extending the longitudinal slit allows the P-type configuration to excite the TM_{010} mode of the SIW resonant cavity, achieving effective radiation in 27 GHz. Simultaneously, to enable dual-band operation in the millimeter-wave frequency range, a smaller-radius semicircular slit is etched within the P-shaped configuration, facilitating effective radiation in another higher frequency band. This design modification enables the antenna to transcend single-band limitations and improves its overall efficiency.

Fig. 6 shows the simulation results of the reflection coefficients of Antenna1, Antenna2, and Antenna3 during the evolution of the antenna unit. It can be seen that Antenna1 is in impedance mismatch and cannot effectively radiate outward. By optimizing the design of the longitudinal slit and circular slit, Antenna2 works in the main mode TM_{010} of the resonant cavity with an operating bandwidth of 26.77 GHz–28.13 GHz and a relative bandwidth of 5%. On the basis of Antenna2, the improved dual P-shaped slit enables Antenna3 to excite a mixed mode with two resonant frequency points of 38.5 GHz and 39.5 GHz, realizing dual-frequency radiation, operating at 26.84–28.15 GHz with a relative bandwidth of 4.8% and 37.77–39.98 GHz with a relative bandwidth of 5.7%.

To further analyze the principle of the designed dual-band antenna, Fig. 5 shows the energy distribution of the antenna electric field at 27.5 GHz, 38.5 GHz, and 39.5 GHz. It can be seen that at 27.5 GHz, the energy mainly gathers around the large semicircular ring slit and longitudinal slit. At 38.5 GHz and 39.5 GHz, the energy is mainly gathered around the small semicircular ring slit and longitudinal slit. It can be seen that the surface currents are directly intercepted by the slot. The large semi-circular gaps and longitudinal gaps produce strong radiation at 27.5 GHz while the small semi-circular gaps and longitudinal gaps produce strong radiation at higher frequencies.

The semicircular slit significantly impacts the perturbation of the electric field distribution and consequently influences the

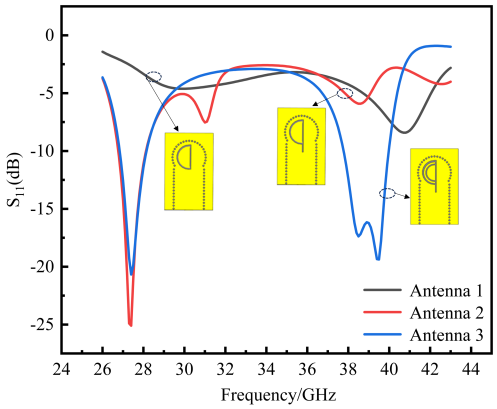

FIGURE 6. The simulation results of the reflection coefficients of Antenna1, Antenna2 and Antenna3.

radiation performance of the antenna. An analysis of the significant parameters of the semicircular slit is conducted. During the parametric analysis, one parameter is systematically varied while keeping all other parameters fixed at the optimal values outlined in Table 1. Fig. 7 illustrates the simulation results of the reflection coefficient for the proposed antenna at various radii (r_1, r_2, r_4, r_5). The analysis of S_{11} curves reveals that changes in r_1 and r_2 impact both operational bands; specifically, increasing r_1 from 2 mm to 2.1 mm shifts the resonance point of the lower band leftwards and widens the operational bandwidth of the higher band. r_2 primarily influences the antenna's impedance matching in both bands. Conversely, alterations in parameters r_4 and r_5 minimally impact the lower frequency band while significantly affecting impedance matching in the higher frequency band.

TABLE 1. Dimensions of the proposed antenna.

Parameters	Values (mm)	Parameters	Values (mm)
p	0.5	r_1	2.05
d	0.3	r_2	1.8
h	0.508	r_3	2.75
s	7	r_4	1.5
n_1	1.4	r_5	1.3
m_1	0.24	W_{siw}	5
dg	4	L_s	18.9
dl	6.15	W_s	20

2.3. Analysis of MIMO Antennas with High Isolation

To achieve MIMO transceiver integration, the previously designed dual-band antennas are consolidated into a two-port MIMO antenna with high isolation. This enhances system capacity by employing MIMO to achieve high-rate, high-quality transmission. In practical implementation, the correlation between the antennas may be relatively large because of the close proximity, and these factors will make the channel capacity of the antenna system deviate from the ideal channel capacity. Therefore, reducing the correlation between antennas is crucial to increasing channel capacity in practical MIMO antenna design.

The inherent structure of SIW provides excellent isolation between antenna units owing to its enclosed metallization aperture. Mutual coupling between MIMO antenna ports is reduced by loading a rectangular slot in the middle of the ground plane to form a DGS. The core principle of defective ground decoupling is to alter current distribution on the antenna surface, minimizing coupling between the antenna ports. Additionally, employing the pattern diversity reduces mutual coupling between units by arranging antenna units relatively parallel, ensuring that each element's radiation direction map does not interfere with others, thereby achieving high isolation between antenna elements. In contrast to other intricate decoupling structures, the proposed MIMO antenna employs solely rectangular slots for the DGS and pattern diversity technique, simplifying the design significantly. The high isolation MIMO antenna structure optimized by HFSS further simulation is shown in Fig. 2. The related parameters are shown in Table 1.

Observing its S_{21} curve in Fig. 8, it is evident that without any decoupling method, the isolation at 38.4–40 GHz consistently exceeds 30 dB, whereas at 26.6–28.2 GHz it is relatively poor. Therefore, the decoupling method is primarily employed to mitigate antenna coupling at 26.6–28.2 GHz and enhance overall antenna's isolation. Compared to the absence of decoupling, the loaded DGS reduces antenna coupling modestly at 26.6–28.2 GHz and significantly between 38.4 GHz and 39.6 GHz, with a slight increase observed from 39.6 GHz to 40.3 GHz. Subsequently, after loading the DGS, the antennas are relatively positioned, resulting in an approximate 3 dB increase in antenna isolation at 26.6–28.2 GHz, maintaining an overall isolation greater than 33 dB. Although isolation slightly decreases from 38.7 to 40.3 GHz, it remains above 33 dB overall. Finally, the combination of the DGS and pattern diversity effectively enhances antenna's isolation, achieving excellent overall isolation.

3. MEASUREMENT RESULTS AND DISCUSSION

The antenna prototype was fabricated, and the sample is shown in Fig. 9. The 2.4 mm coaxial connector has the model number NY24FM0503F04. The antenna was tested using a vector network analyzer from Agilent Technologies, model E8361A. Due to the symmetric characteristic of the proposed MIMO antenna, only 1-port test data is given. Fig. 10(a) presents the S_{11} curves for both simulation and measurement. The measured results indicate that while the trends of the simulated and measured curves are generally consistent across the entire operating frequency band, the measured bandwidth is slightly narrower than the simulated results at lower frequencies (approximately 26.7 GHz to 27.9 GHz) and broader at higher frequencies (approximately 37.95 GHz to 40.92 GHz). The discrepancy between the simulated and measured results may be attributed to the high Q factor of the resonator, minor fabrication deviations, and metal surface roughness which may significantly impact the antenna bandwidth. Additionally, the inclusion of the coaxial connector introduces parasitic parameters, and the

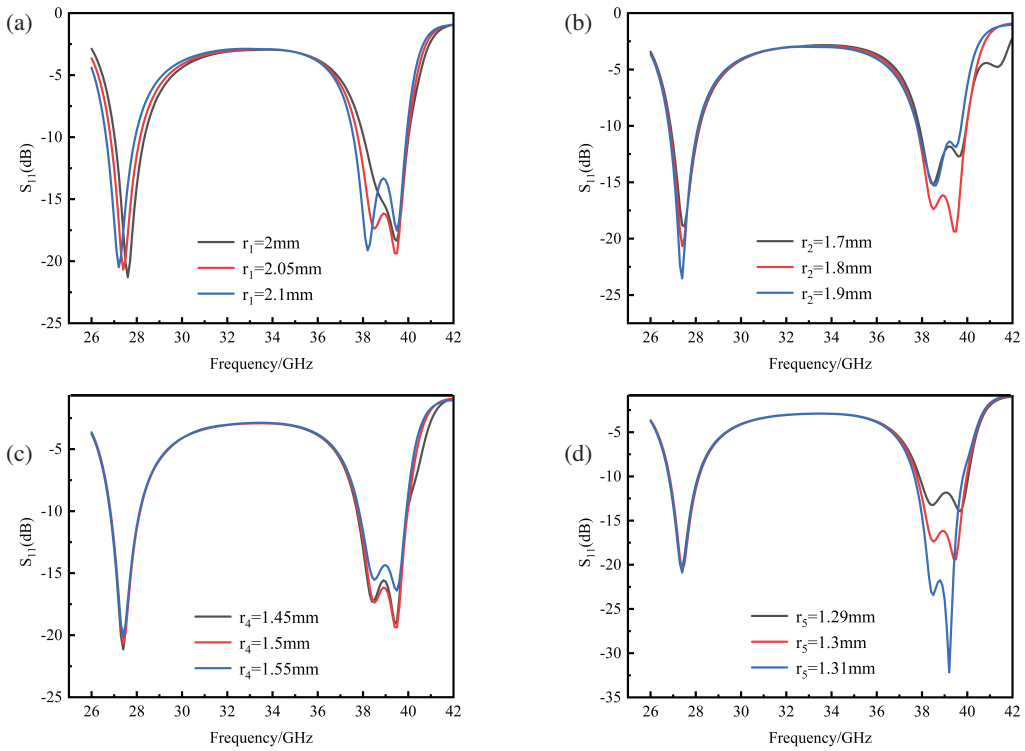

FIGURE 7. The simulation results of the reflection coefficients for different radius (a) r_1; (b) r_2; (c) r_4; (d) r_5.

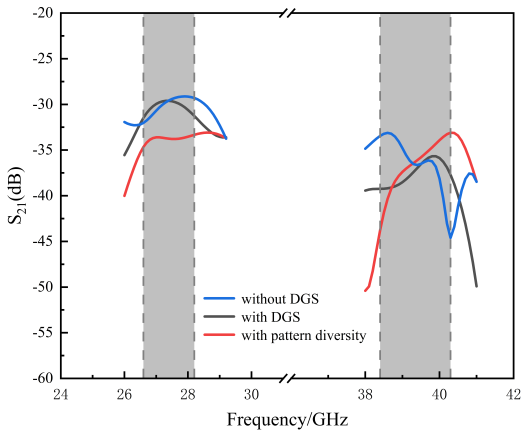

FIGURE 8. S_{21} with different decoupling structures.

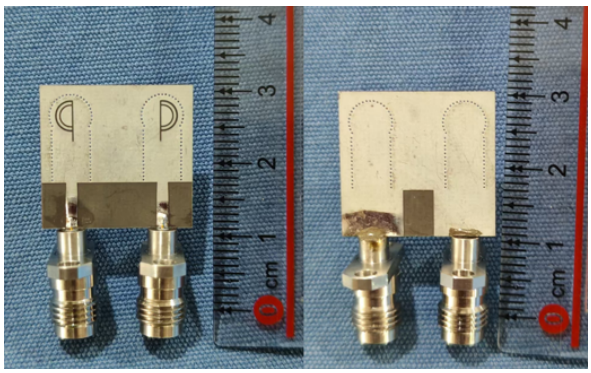

FIGURE 9. Antenna physical picture.

discontinuity between the coaxial and microstrip connections may impact antenna performance.

Figure 11(b) shows the simulated and measured S_{21} and gain curves. Within 26.7–27.9 GHz, the antenna has an isolation of greater than 30 dB, which is approximately 3 dB less than the simulation results. Within the 37.95–40.92 band, the antenna has an excellent isolation of greater than 33 dB. The measured gain is slightly less than the simulated one at 26.7–27.9 GHz, with the peak gain of the antenna recorded at 5.63 dBi. The difference between the simulated and measured gains of the antenna is larger at 37.95–40.92 GHz, with the peak gain reaching 6.35 dBi, which is likely to be caused by the material loss and the drift of the dielectric constant at higher frequencies. Additionally, the coaxial connector may introduce extra losses that could impact antenna performance.

Figure 11 shows the far-field measurement diagram of the antenna in a microwave darkroom. Fig. 12 presents the simulated and measured results for the E-plane and H-plane radiation patterns at three different frequencies. In the two orthogonal planes, the measured and simulated directional maps exhibit a generally consistent trend in the direction of maximum radiation; however, the radiation maps of the antenna show varying degrees of aberration, particularly at higher frequencies where substantial deterioration is evident. Firstly, given the small size of the antenna, the measured directivity maps are influenced by the test conditions and surrounding environment (such as coaxial connectors, cables, and mounting brackets), which contributes to inaccuracies in the results. Secondly, the suboptimal

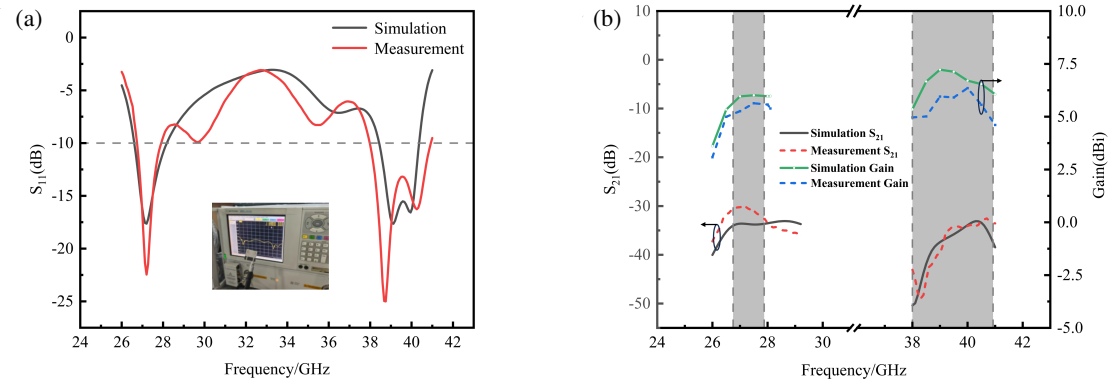

FIGURE 10. Simulated and measured (a) S_{11}; (b) S_{21} and gain.

TABLE 2. Comparison of the proposed antenna with previously reported antennas.

Reference	Port numbers	Frequency/GHz	Gain/dBi	Decoupling method	Isolation/dB	ECC	Size/mm^3
[8]	2	0.81/2.75	−4/2.4	DGS	17	0.21	50 × 100 × 1.56
[9]	4	2.6/5.3	3.98/4.13	Polarization diversity and PSG	21	0.00434	70 × 70 × 1.524
[10]	4	4.43/5.39	6/6.4	Neutralization line	35	0.005	82 × 82 × 1.57
[11]	2	2.4/5.5	3.2/5.8	Shorted edges	20	0.0002	41.9 × 32.3 × 3
[14]	2	28/38	7.1/7.9	Polarization diversity	28	0.0005	20 × 24 × 0.508
[15]	2	27/39	5/5.7	Pattern diversity	25	0.0001	-
This paper	2	27/39	5.63/6.35	Pattern diversity and DGS	30	0.0002	20 × 18.9 × 0.508

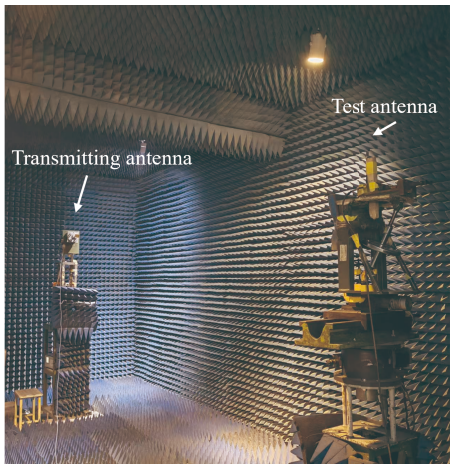

FIGURE 11. The picture of antenna far-field measurement.

radiation characteristics of the directional map at higher frequencies arise because the wavelength decreases with increasing frequency, causing the antenna's physical size to exceed half of the wavelength. Consequently, the antenna cannot retain the characteristics of an electrically small antenna, resulting in noticeable distortion in the directional map.

For MIMO antennas, ECC illustrates the degree of independence of each antenna unit in signal reception; theoretically, ECC should be equal to 0. Diversity gain (DG) indicates the quality and reliability of a MIMO antenna, with an ideal value of 10. For a MIMO antenna with two ports, ECC and DG can be calculated by substituting the S-parameters into Equation (5) and Equation (6) [21]. Fig. 13 shows that the simulated ECC and DG values are less than 0.0002 and greater than 9.995, respectively, over the entire frequency band. This indicates that the antenna meets the MIMO requirements of an ECC value less than 0.5 and a DG close to 10, with good correlation performance and a high degree of independence.

$$ECC = \frac{|S_{11}S_{12}^* + S_{21}S_{22}^*|}{(1-|S_{11}|^2-|S_{21}|^2)(1-|S_{21}|^2-|S_{12}|^2)} \quad (5)$$

$$DG = 10 \times \sqrt{1-|ECC|^2} \quad (6)$$

The dual-band MIMO antenna designed in this paper is compared against key metrics of antennas in the referenced literature, with the results presented in Table 2. Refs. [8–11] implement dual-band MIMO designs below 6 GHz, but the antennas are large and have high profiles, which are not easy to integrate with planar circuits. Refs. [8, 9, 11] also have relatively low gain and isolation. Refs. [14, 15] realize the design of a dual-band MIMO antenna at higher frequencies, but [15] has relatively low gain and isolation. Compared to the proposed antenna, [14] has higher gain but lower isolation and ECC and

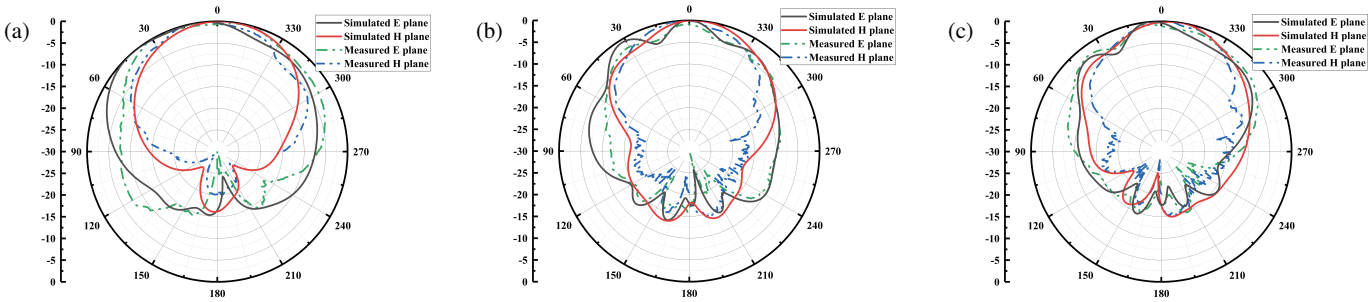

FIGURE 12. Simulated and measured radiation patterns at (a) 27 GHz, (b) 38.5 GHz, (c) 39.5 GHz.

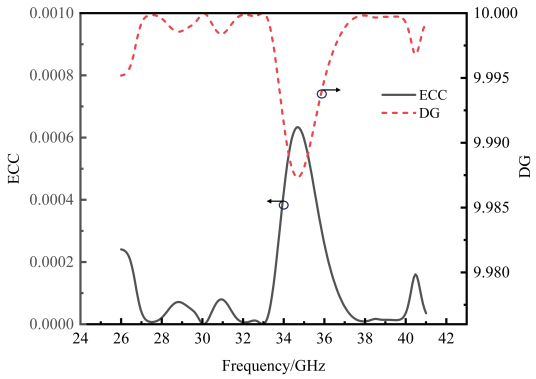

FIGURE 13. ECC and DG for the MIMO antenna.

larger size. In terms of metrics such as antenna size, gain and isolation, the antenna designed in this study outperforms similar models, achieving a compact, dual-band MIMO antenna with high isolation in the millimeter wave band.

4. CONCLUSION

A dual-band MIMO antenna is proposed in this paper which describes the design of the antenna in detail from SIW circular resonant cavity to the proposed antenna and analysis of the operating principle. The improved dual P-shaped antenna generates dual-band radiation at 26.7 GHz–27.9 GHz and 37.95 GHz–40.92 GHz by exciting different resonant modes in the circular resonant cavity. Within the operating frequency bands, peak gains of the antenna are measured at 5.63 dBi and 6.35 dBi, respectively. Pattern diversity and DGS are used to make the isolation of the antenna greater than 30 dB. The ECC is less than 0.0002, and the DG is greater than 9.995, which is close to 10. The developed antenna is ideal for millimeter-wave MIMO communication systems due to its features such as simple structure, compactness, and high isolation.

ACKNOWLEDGEMENT

This work was supported by the Applied Basic Research of Liaoning Province (2022JH2/101300275), Basic Scientific Research Project of Education Department of Liaoning Province (JYTMS20230818), and the National Natural Science Foundation of China (61971210).

REFERENCES

[1] Lockie, D. and D. Peck, "High-data-rate millimeter-wave radios," *IEEE Microwave Magazine*, Vol. 10, No. 5, 75–83, 2009.

[2] Rappaport, T. S., Y. Xing, G. R. MacCartney, A. F. Molisch, E. Mellios, and J. Zhang, "Overview of millimeter wave communications for fifth-generation (5G) wireless networks — With a focus on propagation models," *IEEE Transactions on Antennas and Propagation*, Vol. 65, No. 12, 6213–6230, 2017.

[3] Jemaludin, N. H., A. J. A. Al-Gburi, R. H. Elabd, T. Saeidi, M. F. Akbar, I. M. Ibrahim, and Z. Zakaria, "A comprehensive review on MIMO antennas for 5G smartphones: Mutual coupling techniques, comparative studies, SAR analysis, and future directions," *Results in Engineering*, Vol. 23, 102712, 2024.

[4] Esmail, B. A. F., D. Isleifson, and S. Koziel, "Dual-band millimetre wave MIMO antenna with reduced mutual coupling based on optimized parasitic structure and ground modification," *Scientific Reports*, Vol. 14, No. 1, 20507, 2024.

[5] Gao, M., H. Niu, J. C. Nan, W. H. Liu, and C. L. Liu, "2-port high gain millimeter-wave MIMO antenna for 5G applications," *Progress In Electromagnetics Research M*, Vol. 120, 15–27, 2023.

[6] Cui, L., J. Guo, Y. Liu, and C.-Y.-D. Sim, "An 8-element dual-band MIMO antenna with decoupling stub for 5G smartphone applications," *IEEE Antennas and Wireless Propagation Letters*, Vol. 18, No. 10, 2095–2099, 2019.

[7] Boukarkar, A., X. Q. Lin, Y. Jiang, L. Y. Nie, P. Mei, and Y. Q. Yu, "A miniaturized extremely close-spaced four-element dual-band MIMO antenna system with polarization and pattern diversity," *IEEE Antennas and Wireless Propagation Letters*, Vol. 17, No. 1, 134–137, 2018.

[8] Sharawi, M. S., A. B. Numan, M. U. Khan, and D. N. Aloi, "A dual-element dual-band MIMO antenna system with enhanced isolation for mobile terminals," *IEEE Antennas and Wireless Propagation Letters*, Vol. 11, 1006–1009, 2012.

[9] Malviya, L., R. K. Panigrahi, and M. Kartikeyan, "A 2×2 dual-band MIMO antenna with polarization diversity for wireless applications," *Progress In Electromagnetics Research C*, Vol. 61, 91–103, 2016.

[10] Elobied, A. A., X.-X. Yang, N. Xie, and S. Gao, "Dual-band 2×2 MIMO antenna with compact size and high isolation based on half-mode SIW," *International Journal of Antennas and Propagation*, Vol. 2020, No. 1, 2965767, 2020.

[11] Yan, S., P. J. Soh, and G. A. E. Vandenbosch, "Dual-band textile MIMO antenna based on substrate-integrated waveguide (SIW) technology," *IEEE Transactions on Antennas and Propagation*, Vol. 63, No. 11, 4640–4647, 2015.

[12] Khan, O., S. Khan, S. N. K. Marwat, N. Gohar, M. Bilal, and M. Dalarsson, "A novel densely packed 4×4 MIMO antenna design for UWB wireless applications," *Sensors*, Vol. 23, No. 21, 8888, 2023.

[13] Dubazane, S. P., P. Kumar, and T. J. O. Afullo, "Metasurface superstrate-based MIMO patch antennas with reduced mutual coupling for 5G communications," *The Applied Computational Electromagnetics Society Journal (ACES)*, Vol. 37, No. 4, 408–419, 2022.

[14] Raheel, K., A. Altaf, A. Waheed, S. H. Kiani, D. A. Sehrai, F. Tubbal, and R. Raad, "E-shaped H-slotted dual band mmWave antenna for 5G technology," *Electronics*, Vol. 10, No. 9, 1019, 2021.

[15] Ali, W., S. Das, H. Medkour, and S. Lakrit, "Planar dual-band 27/39 GHz millimeter-wave MIMO antenna for 5G applications," *Microsystem Technologies*, Vol. 27, 283–292, 2021.

[16] Gao, M., C. Liu, J. Nan, and H. Niu, "A broadband SIW cavity-backed circular arc-shaped slot antenna for millimeter-wave applications," *Progress In Electromagnetics Research Letters*, Vol. 117, 47–54, 2024.

[17] Shi, Y., W. J. Wang, and T. T. Hu, "A transparent SIW cavity-based millimeter-wave slot antenna for 5G communication," *IEEE Antennas and Wireless Propagation Letters*, Vol. 21, No. 6, 1105–1109, 2022.

[18] Hong, T., Z. Zhao, W. Jiang, S. Xia, Y. Liu, and S. Gong, "Dual-band siw cavity-backed slot array using TM_{020} and TM_{120} modes for 5G applications," *IEEE Transactions on Antennas and Propagation*, Vol. 67, No. 5, 3490–3495, 2019.

[19] Wu, Q., H. Wang, C. Yu, and W. Hong, "Low-profile circularly polarized cavity-backed antennas using SIW techniques," *IEEE Transactions on Antennas and Propagation*, Vol. 64, No. 7, 2832–2839, 2016.

[20] Ali, M., K. K. Sharma, R. P. Yadav, A. Kumar, F. Jiang, Q. S. Cheng, and G.-L. Huang, "Design of dual mode wideband SIW slot antenna for 5G applications," *International Journal of RF and Microwave Computer-Aided Engineering*, Vol. 30, No. 12, e22449, 2020.

[21] Khalid, M., S. I. Naqvi, N. Hussain, M. Rahman, Fawad, S. S. Mirjavadi, M. J. Khan, and Y. Amin, "4-Port MIMO antenna with defected ground structure for 5G millimeter wave applications," *Electronics*, Vol. 9, No. 1, 71, 2020.